

# LIKO: LiDAR, Inertial, and Kinematic Odometry for Bipedal Robots

Qingrui Zhao<sup>1</sup>, Mingyuan Li<sup>1</sup>, Yongliang Shi<sup>2</sup>, Xuechao Chen<sup>1</sup>, Zhangguo Yu<sup>1</sup>, Lianqiang Han<sup>1</sup>,  
Zhenyuan Fu<sup>1</sup>, Jintao Zhang<sup>1</sup>, Chao Li<sup>1</sup>, Yuanxi Zhang<sup>1</sup>, Qiang Huang<sup>1</sup>

**Abstract**—High-frequency and accurate state estimation is crucial for biped robots. This paper presents a tightly-coupled LiDAR-Inertial-Kinematic Odometry (LIKO) for biped robot state estimation based on an iterated extended Kalman filter. Beyond state estimation, the foot contact position is also modeled and estimated. This allows for both position and velocity updates from kinematic measurement. Additionally, the use of kinematic measurement results in an increased output state frequency of about 1kHz. This ensures temporal continuity of the estimated state and makes it practical for control purposes of biped robots. We also announce a biped robot dataset consisting of LiDAR, inertial measurement unit (IMU), joint encoders, force/torque (F/T) sensors, and motion capture ground truth to evaluate the proposed method. The dataset is collected during robot locomotion, and our approach reached the best quantitative result among other LIO-based methods and biped robot state estimation algorithms. The dataset and source code will be available at <https://github.com/Mr-Zqr/LIKO>.

## I. INTRODUCTION

Biped robots are developing rapidly these days, gradually stepping out of laboratories and into the real world. In contrast to wheeled vehicles or quadrotors that maintain continuous ground contact or experience smooth acceleration patterns, legged robots, especially bipedal ones, encounter intermittent ground contact during locomotion [1]. This introduces additional sensor noise to IMU and joint encoders. Therefore, smooth and precise linear velocity estimation is imperative for stable closed-loop control in bipedal robots [2]. Furthermore, bipedal robots are inherently more prone to instability and falls compared to their quadrupedal counterparts. Consequently, a high-frequency (over 1kHz) controller is essential to ensure stability in balance and gait control [3], [4]. Similarly, the state estimator should also be high-frequency (250Hz to 1kHz) and globally accurate to enable the formation of a stable feedback control system [5].

Existing state estimation algorithms for legged robots mainly use proprioceptive sensors, such as IMUs, joint encoders, and contact sensors. These sensor measurements are fused using filtering-based methods, such as unscented Kalman filter [6], extended Kalman filter [7], and invariant extended Kalman filter (InEKF) [8]. These methods enable real-time and high-frequency state estimation. However, according to [6], the robot’s global position and yaw angle can-

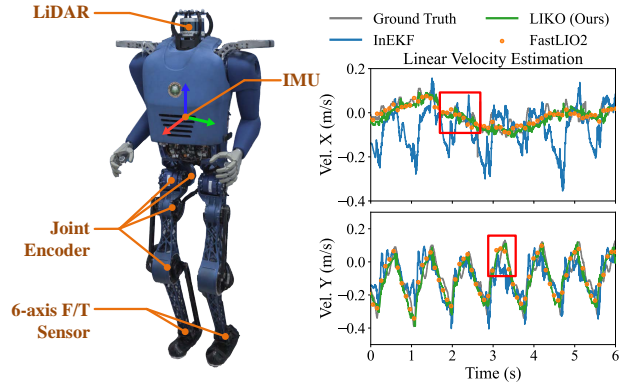


Fig. 1. *Left*: The proposed LIKO state estimation system is tested on a BHR-B3 biped robot. The robot’s body coordinate is aligned with the IMU coordinate. *Right*: Linear velocity estimation comparison between proposed LIKO (green), Inertial Kinematic odometry Contact-aided InEKF [8] (blue), and LiDAR-Inertial odometry (LIO) FastLIO2 [9] (orange) against ground truth (gray). The velocity estimated by FastLIO2 is plotted in scatter form since its update frequency is at 10Hz with Velodyne LiDAR, while other methods operate at 1kHz. The red boxes highlighted where the proposed method exhibits more accurate velocity estimation than others.

not be observed using only proprioceptive sensors, resulting in drift.

To mitigate the position drift and make full use of the environmental information, some legged robots are equipped with exteroceptive sensors, namely stereo cameras and LiDARs. The introduction of these sensors also comes with a large computation load. To manage this computational load without sacrificing real-time performance, the loosely coupled approach has been employed [5]. However, this method solely relies on the estimated state from each sensor and lacks the capability for online estimation of sensor parameters, leading to suboptimal state estimation. Recently, a tightly coupled method has also been presented [1], which tightly fuses visual, inertial, LiDAR, and kinematic measurements through factor graphs. However, it is designed for quadruped robots and does not include foothold estimation.

To address the above limitations, we present LiDAR-Inertial-Kinematic Odometry (LIKO), a tightly-coupled high-frequency and accurate odometry for biped robot state estimation. As shown in Fig. 1, our method achieved high-frequency, smooth, and accurate velocity estimation against other state-of-the-art state estimation algorithms for biped robots and LiDAR-inertial odometry. More specifically, our contributions are as follows:

- LIKO: a tightly-coupled LiDAR-Inertial-Kinematic Odometry to achieve high-frequency and accurate state

\*This work was supported in part by the National Natural Science Foundation of China under Grant 62073041, Grant 62088101, and the Beijing Municipal Science and Technology Project under Grant Z231100007123006.

<sup>1</sup>School of Mechatronic Engineering, Beijing Institute of Technology (BIT), Beijing, China. Contact: chenxuechao@bit.edu.cn

<sup>2</sup>Qiyuan Lab

estimation for biped robots.

- Online estimation of the foot contact position, leveraging both position and velocity from the leg odometry as the measurement update of the state.
- Datasets containing multiple motion patterns of a biped robot and corresponding motion-captured ground truth are collected and announced to test LIKO.
- Experimental validations were conducted on hardware and provided datasets to assess the performance of the proposed algorithm. The results demonstrated a 14% improvement in accuracy compared to the current state-of-the-art methods.

## II. RELATED WORKS

### A. Biped Robot State Estimation

Many legged robot state estimation algorithms focus on fusing IMU and kinematic measurements using filter-based methods. Kinematic measurements, commonly referred to as leg odometry [5], leverage joint encoders and contact sensors, typically F/T sensors, in conjunction with robot forward kinematics to derive position and velocity information under the non-slipping assumption [10], [11]. Bloesch *et al.* [6] introduced the application of an Unscented Kalman filter to robot state estimation. Hartley *et al.* [8] proved that the system dynamics of bipedal robots satisfy the group affine property, leading to the introduction of a contact-aided InEKF for better convergence in orientation estimation. However, the leg odometry in this work is limited to using only position measurements. Xavier *et al.* [12] modeled the contact velocity by attaching additional IMUs to robot feet, which released the non-slipping assumption and achieved better performance in long-term experiments. Nonetheless, as demonstrated in [6], solely relying on proprioceptive sensors results in the non-observability of global position and yaw angle, leading to position drift.

To address the position drift problem and make full use of the environmental information, some legged robots also use exteroceptive sensors, such as stereo cameras and LiDARs [13]–[16]. Camurri *et al.* [5] used an extended Kalman filter (EKF) to loosely-couple estimations from visual, inertial, LiDAR, and leg odometry. Wisth *et al.* [1] proposed VILENS, which tightly coupled all sensor modalities mentioned above with a factor graph. However, since the factor graph optimizes a large number of states at a time, this method is computationally intensive by nature. Fallon *et al.* [14] used EKF in conjunction with IMU, joint encoder, and LiDAR to estimate the state of the Atlas robot. However, it did not include contact position estimation. The leg odometry only provides linear velocity measurement by taking the derivative of forward kinematics.

### B. LiDAR-Inertial Odometry

LiDAR odometry entails the estimation of a robot’s pose and position through LiDAR sensors. This is achieved by determining the relative transformation between two consecutive sensor frames with scan-matching techniques such

as the Iterative Closest Point (ICP) [17] or Generalized-ICP (GICP) [18]. Recently, some feature-based approaches [19]–[21] have been reported, which selectively use the most salient data points to perform the scan-matching algorithm. However, the presence of noise stemming from LiDAR’s rotation mechanism and sensor movements during scanning often introduces distortions in the acquired point clouds. Thus, relying solely on LiDAR for state estimation is not ideal, as registering distorted point clouds can lead to cumulative errors, ultimately resulting in odometry drift.

IMU is commonly employed to address such challenges, forming LiDAR-Inertial odometry (LIO). Loosely-coupled LIO typically processes LiDAR and IMU measurements separately and fuses them using a Kalman filter. In LeGO-LOAM [20], IMU measurements are utilized for de-skewing lidar scans and providing motion prior to scan-matching. Conversely, tightly-coupled LIO systems generally utilize raw LiDAR data in conjunction with IMU data. FAST-LIO series [9], [22] employed an Iterated Extended Kalman Filter (IEKF) to fuse LiDAR and IMU measurements. Additionally, they introduced a back-propagation approach to estimate the relative motion between the sample time of each point and the scan end time. Recently, DLIO [23] introduced a coarse-to-fine motion correction method and a hierarchical geometric observer [24] for data fusion.

## III. METHODOLOGY

We begin by introducing the relevant notation and conventions. In general, we denote scalars and frame abbreviations in lowercase italics, matrices in uppercase Roman bold, and vectors in lowercase Roman bold. The operator  $[\mathbf{a}]_{\wedge}$  is used to convert a vector  $\mathbf{a}$  into its corresponding skew-symmetric matrix. We also use  $\mathbf{x}$ ,  $\hat{\mathbf{x}}$ , and  $\hat{\mathbf{x}}^j$  to represent the ground-truth, propagated, and updated values of  $\mathbf{x}$  respectively. The notation  $\hat{\mathbf{x}}^j$  denotes the  $j$ -th update of  $\mathbf{x}$  in the IEKF.  $\boxplus$  and  $\boxminus$  are two encapsulation operators that represent a bijective mapping from a local neighborhood on  $\mathcal{M}$  to its tangent space  $\mathbb{R}^n$  [22]. Besides,  $\tilde{\mathbf{x}}$  represents the discrepancy between  $\mathbf{x}$  and  $\hat{\mathbf{x}}$ , and  $(\cdot)^m$  stands for sensor measurements.

### A. System Overview

The overview of the presented state estimation system is shown in Fig. 2. The system receives input from a LiDAR, an IMU, joint encoders, and F/T sensors. Acceleration and angular velocity measurements from the IMU are first integrated to produce state propagation. The propagated states are then updated in IEKF using Robot Kinematics and LiDAR measurements. In Robot Kinematics measurement, F/T sensors determine which foot is in contact with the ground. Thereafter, the robot’s position and linear velocity are computed, integrating data from joint encoders, foothold estimation, and forward kinematic introduced in Section III-E. Meanwhile, LiDAR points of a scan are accumulated and fed into the distortion correction module with IMU measurements for motion compensation. The rectified point cloud is then used as a LiDAR measurement. The IEKF-

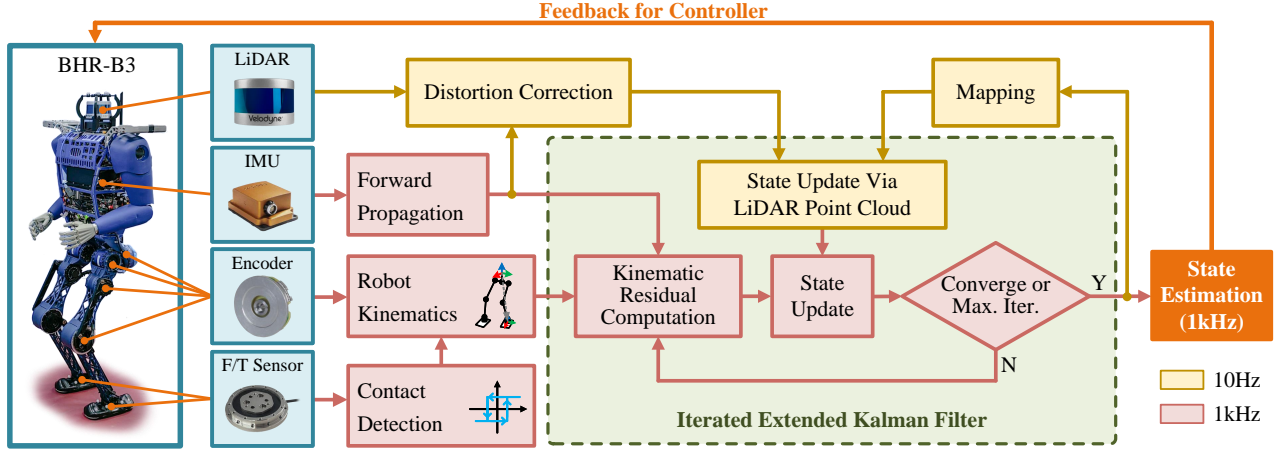


Fig. 2. System overview of LIKO. The system receives input from a LiDAR, an IMU, joint encoders, and F/T sensors. The IMU is used for state propagation, while LiDAR, joint encoder, and F/T sensors generate three different types of state measurement. The formulation of the iterated Kalman filter is discussed in Section III.

updated state is then used for the control module and point cloud registration.

### B. State Representation

The robot state  $\mathbf{x}$  is defined as follows:

$$\mathbf{x} \triangleq [{}^G\mathbf{R}_I \quad {}^G\mathbf{p}_I^T \quad {}^G\mathbf{v}_I^T \quad \mathbf{b}^\omega^T \quad \mathbf{b}^a^T \quad {}^G\mathbf{p}_c^T \quad {}^G\mathbf{g}^T]^T$$

$$\mathcal{M} = SO(3) \times \mathbb{R}^{18}, \quad \mathbf{x} \in \mathcal{M} \quad (1)$$

where  ${}^G\mathbf{R}_I \in SO(3)$ ,  ${}^G\mathbf{p}_I \in \mathbb{R}^3$ ,  ${}^G\mathbf{v}_I \in \mathbb{R}^3$  are orientation, position, and velocity of the IMU with respect to the global frame, respectively.  $\mathbf{b}^\omega, \mathbf{b}^a \in \mathbb{R}^3$  are random walk biases of the IMU gyroscope and accelerometer;  ${}^G\mathbf{p}_c \in \mathbb{R}^3$  is the contact position of the robot in the global frame, and  ${}^G\mathbf{g} \in \mathbb{R}^3$  is the gravity vector in the global frame.

The IMU measurements are modeled as real values corrupted by additive Gaussian white noise ( $\mathbf{w}^\omega, \mathbf{w}^a$ ) and random walk bias ( $\mathbf{b}^\omega, \mathbf{b}^a$ ):

$$\boldsymbol{\omega}^m = \boldsymbol{\omega} + \mathbf{w}^\omega + \mathbf{b}^\omega, \quad \mathbf{a}^m = \mathbf{a} + \mathbf{w}^a + \mathbf{b}^a \quad (2)$$

### C. Propagation Model

The kinematic model of the state  $\mathbf{x}$  can be written as:

$$\begin{aligned} {}^G\dot{\mathbf{R}}_I^T &= {}^G\mathbf{R}_I [\boldsymbol{\omega}^m - \mathbf{b}^\omega - \mathbf{w}^\omega]_\wedge \\ {}^G\dot{\mathbf{p}}_I &= {}^G\mathbf{v}_I \\ {}^G\dot{\mathbf{v}}_I &= {}^G\mathbf{R}_I (\mathbf{a}^m - \mathbf{b}^a - \mathbf{w}^a) + {}^G\mathbf{g} \\ \dot{\mathbf{b}}^\omega &= \mathbf{w}^{b\omega}, \quad \dot{\mathbf{b}}^a = \mathbf{w}^{ba} \\ {}^G\dot{\mathbf{p}}_c &= {}^G\mathbf{R}_I \cdot \mathbf{fko}(\mathbf{q}) \cdot \mathbf{w}^c, \quad {}^G\dot{\mathbf{g}} = \mathbf{0} \end{aligned} \quad (3)$$

where  $\mathbf{fko}(\mathbf{q})$  is the orientation of the contact frame with respect to the IMU frame computed through encoder measurements,  $\mathbf{q} \in \mathbb{R}^M$ , and the forward kinematics. Besides, we relax the static contact assumption by adding a contact noise  $\mathbf{w}^c$ . The continuous kinematic model in (3) can be discretized at each imu measurement  $t$ , with period  $\Delta t$ :

$$\mathbf{x}_{t+1} = \mathbf{x}_t \boxplus (\Delta t \mathbf{f}(\mathbf{x}_t, \mathbf{u}_t, \mathbf{w}_t)) \quad (4)$$

the function  $\mathbf{f}$ , input  $\mathbf{u}$ , and noise  $\mathbf{w}$  are defined as below:

$$\mathbf{f}(\mathbf{x}_t, \mathbf{u}_t, \mathbf{w}_t) = \begin{bmatrix} \boldsymbol{\omega}_t^m - \mathbf{b}_t^\omega - \mathbf{w}_t^\omega \\ {}^G\mathbf{v}_{I_t} \\ {}^G\mathbf{R}_{I_t} (\mathbf{a}_t^m - \mathbf{b}_t^a - \mathbf{w}_t^a) + {}^G\mathbf{g}_t \\ \mathbf{w}_t^{b\omega} \\ \mathbf{w}_t^{ba} \\ {}^G\mathbf{R}_{I_t} \cdot \mathbf{fko}(\mathbf{q}_t) \cdot \mathbf{w}_t^c \\ \mathbf{0}_{3 \times 1} \end{bmatrix}$$

$$\mathbf{u} \triangleq [\boldsymbol{\omega}^{mT} \quad \mathbf{a}^{mT}]^T$$

$$\mathbf{w} \triangleq [\mathbf{w}^{\omega T} \quad \mathbf{w}^{aT} \quad \mathbf{w}^{b\omega T} \quad \mathbf{w}^{baT} \quad \mathbf{w}^{cT}]^T \quad (5)$$

The forward propagation of the state  $\mathbf{x}_t$  follows (4) by setting  $\mathbf{w}_t = \mathbf{0}$ :

$$\tilde{\mathbf{x}}_t = \hat{\mathbf{x}}_{t-1} \boxplus (\Delta t \mathbf{f}(\hat{\mathbf{x}}_{t-1}, \mathbf{u}_t, \mathbf{0})) \quad (6)$$

and the covariance propagation:

$$\check{\mathbf{P}}_t = \mathbf{F}_{\tilde{\mathbf{x}}} \hat{\mathbf{P}}_{t-1} \mathbf{F}_{\tilde{\mathbf{x}}}^T + \mathbf{F}_w \mathbf{Q} \mathbf{F}_w^T \quad (7)$$

where  $\mathbf{F}_{\tilde{\mathbf{x}}}$  and  $\mathbf{F}_w$  are partial differentiation of  $\tilde{\mathbf{x}}_t$  with respect to  $\tilde{\mathbf{x}}_{t-1}$  and  $\mathbf{w}_{t-1}$  separately.

Notice that  $\check{\mathbf{P}}_t$  represents the covariance of the following error state:

$$\mathbf{x}_t \boxminus \tilde{\mathbf{x}}_t = \hat{\mathbf{x}}_t^j \boxminus \tilde{\mathbf{x}}_t + \mathbf{J} \tilde{\mathbf{x}}_t \sim \mathcal{N}(\mathbf{0}, \check{\mathbf{P}}_t) \quad (8)$$

where the right superscript  $j$  stands for the  $j$ -th update in the iterated Kalman filter,  $\mathbf{J}$  is the partial differentiation of  $\mathbf{x}_t \boxminus \tilde{\mathbf{x}}_t$  with respect to  $\tilde{\mathbf{x}}_t$  evaluated at zero:

$$\mathbf{J} = \begin{bmatrix} \mathbf{A} \left( {}^G\hat{\mathbf{R}}_I^j \boxminus {}^G\check{\mathbf{R}}_I \right)^{-T} & \mathbf{0}_{3 \times 18} \\ \mathbf{0}_{18 \times 3} & \mathbf{I}_{18 \times 18} \end{bmatrix}$$

$$\mathbf{A}(\mathbf{u})^{-1} = \mathbf{I} - \frac{[\mathbf{u}]_\wedge}{2} + \left( 1 - \frac{\|\mathbf{u}\|}{2} \cot \left( \frac{\|\mathbf{u}\|}{2} \right) \right) \frac{[\mathbf{u}]_\wedge}{\|\mathbf{u}\|} \quad (9)$$

#### D. LiDAR Measurement

We model the LiDAR measurements the same way as in [22]. The  $j$ -th point in scan  $k$  at the LiDAR frame is noted as  ${}^L p_j$ . After distortion correction using the IMU back-propagation, all feature points in scan  $t_k$  are mapped to the scan end time  $t_k$ . Meanwhile, each feature point corresponds to a plane feature in the global map. The residual of LiDAR measurement is defined as:

$$\begin{aligned} \mathbf{0} &= \mathbf{h}_j(\mathbf{x}_t, {}^L \mathbf{n}_j) \\ &= \mathbf{u}_j^T \left( {}^G \mathbf{T}_{I_k} {}^I \mathbf{T}_L ({}^L \mathbf{p}_j + {}^L \mathbf{n}_j) - {}^G \mathbf{q}_j \right) \end{aligned} \quad (10)$$

where  $\mathbf{u}_j$  is the normal vector of the corresponding plane,  ${}^G \mathbf{q}_j$  is the point on the corresponding plane,  ${}^G \mathbf{T}_{I_k}$  is the relative pose between world frame and local frame,  ${}^I \mathbf{T}_L$  is extrinsic, and  ${}^L \mathbf{n}_j$  is the LiDAR ranging and beam-directing noise.

Moreover, approximating the measurement equation (10) by its first-order approximation at  $\tilde{\mathbf{x}}_t$  leads to:

$$\begin{aligned} \mathbf{0} &= \mathbf{h}_j(\mathbf{x}_t, {}^L \mathbf{n}_j) \\ &\simeq \mathbf{h}_j(\tilde{\mathbf{x}}_t, \mathbf{0}) + \mathbf{H}_j \tilde{\mathbf{x}}_t + \mathbf{r}_j \end{aligned} \quad (11)$$

where  $\tilde{\mathbf{x}}_t = \mathbf{x}_t \boxminus \hat{\mathbf{x}}_t$  is the state error,  $\mathbf{r}_j \sim \mathcal{N}(\mathbf{0}, \mathbf{R}_j)$  is the noise of Gaussian distribution due to the raw LiDAR measurement  ${}^L \mathbf{n}_j$ , and  $\mathbf{H}_j$  is the Jacobian matrix of the measurement model with respect to  $\tilde{\mathbf{x}}_t$ , evaluated at zero, which is given as:

$$\begin{aligned} \mathbf{H}_j &= \left. \frac{\partial \mathbf{h}_j(\tilde{\mathbf{x}}_t \boxplus \hat{\mathbf{x}}_t, \mathbf{0})}{\partial \tilde{\mathbf{x}}_t} \right|_{\tilde{\mathbf{x}}_t=\mathbf{0}} \\ &= \mathbf{u}_j^T \left[ -{}^G \tilde{\mathbf{R}}_I \left[ {}^I \mathbf{R}_L {}^L \mathbf{p}_j + {}^I \mathbf{t}_L \right]_{\wedge} \quad \mathbf{I}_{3 \times 3} \quad \mathbf{0}_{3 \times 12} \right] \end{aligned} \quad (12)$$

#### E. Kinematic Measurement

1) *Contact Classification*: The biped robot platform used in this work is equipped with F/T sensors at both feet. The contact state can be inferred by thresholding the measured normal force at 250 N. Additionally, we applied a Schmitt trigger to filter contact states to deal with noisy force sensor measurements.

2) *Velocity Measurement*: The position of the foot in contact with the ground can be written as:

$${}^G \mathbf{p}_{foot} = {}^G \mathbf{R}_I \cdot \mathbf{fk}(\mathbf{q}) + {}^G \mathbf{p}_I \quad (13)$$

where  $\mathbf{q}$  are the joint positions and  $\mathbf{fk}(\mathbf{q})$  is the forward kinematics function.

The linear velocity of the robot's floating base at time  $t$  expressed in the global frame can be computed by taking the derivative of (13) and assuming that the foot velocity is zero:

$${}^G \mathbf{v}_I = -{}^G \mathbf{R}_I (\mathbf{J}(\mathbf{q}) \dot{\mathbf{q}} + \boldsymbol{\omega}_t \times \mathbf{fk}(\mathbf{q})) \quad (14)$$

where  $\mathbf{J}(\mathbf{q})$  is the corresponding kinematic Jacobian. Both the joint positions and velocities are measured from encoders and corrupted by additive zero-mean Gaussian noise  $\mathbf{w}^q$  and  $\mathbf{w}^{\dot{q}}$ :

$$\mathbf{q}^m = \mathbf{q} + \mathbf{w}^q, \quad \dot{\mathbf{q}}^m = \dot{\mathbf{q}} + \mathbf{w}^{\dot{q}} \quad (15)$$

After substituting (15) into (14), we can formulate the measurement of base velocity:

$$\begin{aligned} {}^G \mathbf{v}_I^m &= -{}^G \mathbf{R}_I \left( \mathbf{J}(\mathbf{q}^m - \mathbf{w}^q) \cdot (\dot{\mathbf{q}}^m - \mathbf{w}^{\dot{q}}) + \right. \\ &\quad \left. (\boldsymbol{\omega}_t^m - \mathbf{b}_\omega) \times \mathbf{fk}(\mathbf{q}^m - \mathbf{w}^q) \right) \end{aligned} \quad (16)$$

The velocity residual  $\mathbf{r}_{cv}(\tilde{\mathbf{x}}_t, \mathbf{u}_t, \mathbf{q}, \dot{\mathbf{q}})$  is defined as:

$$\mathbf{r}_{cv}(\tilde{\mathbf{x}}_t, \mathbf{u}_t, \mathbf{q}, \dot{\mathbf{q}}) = \mathbf{z}_{cv} = {}^G \tilde{\mathbf{v}}_I - {}^G \mathbf{v}_I^m \quad (17)$$

where  ${}^G \tilde{\mathbf{v}}_I$  is the propagated base velocity from IMU propagation process.

Then, we obtain the first-order Taylor expansion of the true zero residual  $\mathbf{r}_{cv}(\mathbf{x}_t, \mathbf{u}_t, \mathbf{q}, \dot{\mathbf{q}})$  as:

$$\begin{aligned} \mathbf{0} &= \mathbf{h}_{cv}(\mathbf{x}_t, \mathbf{u}_t, \mathbf{w}^q, \mathbf{w}^{\dot{q}}) \\ &\simeq \mathbf{h}_{cv}(\tilde{\mathbf{x}}_t, \mathbf{u}_t, \mathbf{0}, \mathbf{0}) + \mathbf{H}_{cv} \tilde{\mathbf{x}}_t + \mathbf{w}_{cv} \\ &= \mathbf{z}_{cv} + \mathbf{H}_{cv} \tilde{\mathbf{x}}_t + \mathbf{w}_{cv} \end{aligned} \quad (18)$$

where  $\mathbf{w}_{cv} \sim \mathcal{N}(\mathbf{0}, \boldsymbol{\Sigma}_{cv})$  and

$$\begin{aligned} \mathbf{H}_{cv} &= \left. \frac{\partial \mathbf{r}(\tilde{\mathbf{x}}_t \boxplus \hat{\mathbf{x}}_t, \mathbf{u}_t, \mathbf{q}, \dot{\mathbf{q}})}{\partial \tilde{\mathbf{x}}_t} \right|_{\tilde{\mathbf{x}}_t=\mathbf{0}} \\ &= [\mathbf{H}_{cv1} \quad \mathbf{0}_{3 \times 3} \quad \mathbf{I}_3 \quad {}^G \tilde{\mathbf{R}}_I [\mathbf{fk}(\mathbf{q})]_{\wedge} \quad \mathbf{0}_{3 \times 9}] \\ \mathbf{H}_{cv1} &= {}^G \tilde{\mathbf{R}}_I [\mathbf{J}(\mathbf{q}) \dot{\mathbf{q}} + (\boldsymbol{\omega}_t - \mathbf{b}^\omega \times \mathbf{fk}(\mathbf{q}))]_{\wedge} \end{aligned} \quad (19)$$

3) *Position Measurement*: The position residual measured from contact and forward kinematics can be written as:

$$\mathbf{z}_{cp} = {}^G \tilde{\mathbf{p}}_c - {}^G \tilde{\mathbf{p}}_I - {}^G \tilde{\mathbf{R}}_I \cdot \mathbf{fk}(\mathbf{q}) \quad (20)$$

Similarly, substituting (15) into (20) results in position measurement residual:

$$\begin{aligned} \mathbf{0} &= \mathbf{h}_{cp}(\mathbf{x}_t, \mathbf{u}_t, \mathbf{w}^q) \\ &= \mathbf{h}_{cp}(\tilde{\mathbf{x}}_t, \mathbf{u}_t, \mathbf{0}) + \mathbf{H}_{cp} \tilde{\mathbf{x}}_t + \mathbf{w}_{cp} \\ &= \mathbf{z}_{cp} + \mathbf{H}_{cp} \tilde{\mathbf{x}}_t + \mathbf{w}_{cp} \end{aligned} \quad (21)$$

where  $\mathbf{w}_{cp} \sim \mathcal{N}(\mathbf{0}, \boldsymbol{\Sigma}_{cp})$  and

$$\mathbf{H}_{cp} = [{}^G \tilde{\mathbf{R}}_I [\mathbf{fk}(\mathbf{q})]_{\wedge} \quad -\mathbf{I}_3 \quad \mathbf{0}_{3 \times 9} \quad \mathbf{I}_3 \quad \mathbf{0}_{3 \times 3}] \quad (22)$$

#### F. State Update

Combining the prior in (4) with the measurement model from (11), (18), and (21) yields the maximum a-posteriori (MAP) estimation:

$$\begin{aligned} \min_{\tilde{\mathbf{x}}_t} &\left( \|\mathbf{x}_t \boxminus \hat{\mathbf{x}}_t\|_{\mathbf{P}_t^{-1}}^2 + \sum_{j=1}^m \|\mathbf{h}_j + \mathbf{H}_j \tilde{\mathbf{x}}_t\|_{\mathbf{R}_j^{-1}}^2 + \right. \\ &\quad \left. \|\mathbf{h}_{cv}(\tilde{\mathbf{x}}_t, \mathbf{u}_t, \mathbf{0}, \mathbf{0}) + \mathbf{H}_{cv} \tilde{\mathbf{x}}_t\|_{\boldsymbol{\Sigma}_{cv}^{-1}}^2 + \right. \\ &\quad \left. \|\mathbf{h}_{cp}(\tilde{\mathbf{x}}_t, \mathbf{u}_t, \mathbf{0}) + \mathbf{H}_{cp} \tilde{\mathbf{x}}_t\|_{\boldsymbol{\Sigma}_{cp}^{-1}}^2 \right) \end{aligned} \quad (23)$$

Denote:

$$\begin{aligned} \mathbf{H} &= [\mathbf{H}_1^T, \dots, \mathbf{H}_j^T, \mathbf{H}_{cv}, \mathbf{H}_{cp}]^T \\ \mathbf{R} &= \text{diag}(\mathbf{R}_1, \dots, \mathbf{R}_j, \boldsymbol{\Sigma}_{cv}, \boldsymbol{\Sigma}_{cp}) \\ \mathbf{z}_t &= [\mathbf{h}_1(\tilde{\mathbf{x}}_t, \mathbf{0}), \dots, \mathbf{h}_j(\tilde{\mathbf{x}}_t, \mathbf{0}), \mathbf{h}_{cv}, \mathbf{h}_{cp}]^T \\ \mathbf{P} &= \tilde{\mathbf{P}}_t \end{aligned} \quad (24)$$

TABLE I  
SENSOR SPECIFICATIONS OF THE BHR-B3 ROBOT

Sensor	Model	Hz	Specs
Encoder	HEIDENHAIN EBI-1135	1000	Res: < 0.0014°
F/T Sensor	SRI M3714B4	1000	Capacity: x, y : 900N, 100Nm z : 1800N, 100Nm
LiDAR	Velodyne VLP-16	10	Res: 16px × 1824px
IMU	Xsens Mti-100	200	Init Bias: 0.2°/s   5mg Bias Stab: 10°/h   15mg

Following [22], the Kalman gain is computed as:

$$\mathbf{K} = (\mathbf{H}^T \mathbf{R}^{-1} \mathbf{H} + \mathbf{P}^{-1})^{-1} \mathbf{H}^T \mathbf{R}^{-1} \quad (25)$$

Then we can update the state estimate as:

$$\hat{\mathbf{x}}_t^{j+1} = \hat{\mathbf{x}}_t^j \boxplus \left( -\mathbf{K} \mathbf{z}_t^j - (\mathbf{I} - \mathbf{K} \mathbf{H})(\mathbf{J})^{-1} \left( \hat{\mathbf{x}}_t^j \boxminus \tilde{\mathbf{x}}_t \right) \right) \quad (26)$$

The above process is iterated until convergence (i.e., the update is smaller than a given threshold). Then, the optimal estimation and covariance is:

$$\hat{\mathbf{x}}_t = \hat{\mathbf{x}}_t^{j+1}, \quad \hat{\mathbf{P}} = (\mathbf{I} - \mathbf{K} \mathbf{H}) \mathbf{P} \quad (27)$$

#### IV. EXPERIMENTS

Inspired by FastLIO2 [9], we achieved the C++ implementation of LIKO. The experiment and datasets were conducted on the BHR-B3 bipedal robot (shown in Fig. 1) using a walking controller from [25]. The robot was controlled by an Intel NUC with AMD Ryzen 7 5700u and 16 GiB RAM. The sensor specifications of BHR-B3 are shown in Table I. A more detailed introduction of BHR-B3 is presented in [26]. The IMU, joint encoder, and F/T sensor are connected to the NUC via EtherCAT, while the LiDAR is connected using Ethernet. Additionally, we use Pinocchio [27] for kinematic computation.

##### A. Dataset

In this section, we introduce the dataset used to evaluate LIKO. The dataset was collected in a room equipped with a VICON MoCap system, where the BHR-B3 robot walked in different patterns. The LiDAR, IMU, F/T sensor, joint encoder, and VICON MoCap measurements are collected in the format of ROS bags [28]. The VICON MoCap measurement is the ground truth in each dataset. Motion patterns performed in each dataset are listed as follows:

- *forward\_backward*: The robot walks forward in a straight line and then reverses backward to the start point.
- *square\_walk*: The robot walks along a square trajectory with a side length of about three meters, starting from the center of the square and returning to the center.
- *square\_walk\_dynamic*: The robot follows the same trajectory as in *square\_walk*, but returns to the center from another side.

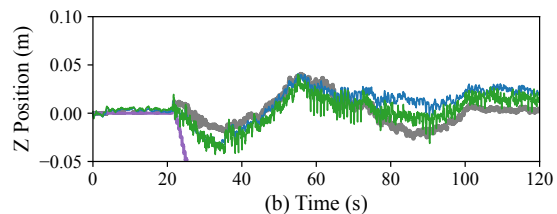
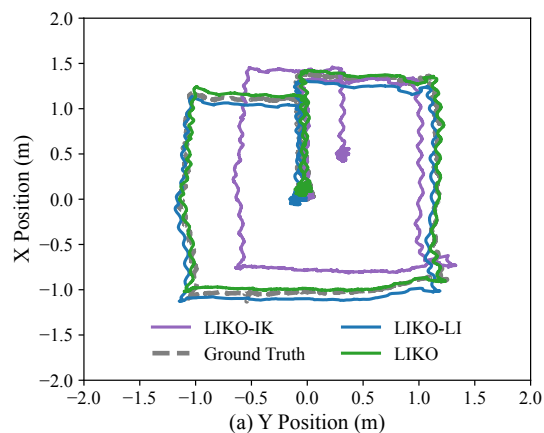


Fig. 3. *Top*: XY position trajectory estimation results of three LIKO variants used in the ablation study against ground truth (gray). *Bottom*: The Z Position trajectory estimation results of three LIKO variants used in the ablation study against ground truth (gray).

- *walk\_in\_place*: The robot walks in place and rotates 90 degrees counterclockwise.
- *up\_slope*: The robot walks up a slope, stays at the top for a short time and then walks downward.

##### B. Ablation Study

In this section, we study the individual contribution of different sensor modalities. The set of combinations tested are as follows: 1) LIKO-IK: IMU and leg odometry are used. In this way, LIKO-IK is a proprioceptive odometry that uses IEKF for sensor fusion. 2) LIKO-LI: LiDAR and IMU are used. This is similar to FastLIO2 but the odometry output frequency is 1kHz. 3) LIKO: uses LiDAR, IMU, and leg odometry.

We used the *square\_walk* dataset for the ablation study, the result is shown in Fig. 3. Note that LIKO-LI has performance closer to LIKO than LIKO-IK. This suggests that the LiDAR sensor plays the main contribution in global position estimation. Although LIKO-IK drifts in position estimation, the high-frequency nature of leg odometry allows it to provide velocity measurements more timely and accurately than LIO methods.

##### C. Comparison With Other Algorithms

1) *Comparison with LIO algorithms*: This section compares the LIKO against state-of-the-art LiDAR-Inertial mapping systems, including FastLIO2 [9], LIO-SAM [29] and LINS [30]. We use the absolute pose error (APE) as an accuracy indicator for whole trajectories and a translational relative pose error (RPE) for drift evaluation. Both APE and RPE are evaluated using evo [31].



TABLE II  
ACCURACY EVALUATION (RMSE) IN SEQUENCES WITH GROUND TRUTH

Algorithm	<i>forward_backward</i>		<i>square_walk</i>		<i>square_walk_long</i>		<i>walk_in_place</i>		<i>up_slope</i>		Frequency (Hz)
	APE (m)	RPE(%)	APE (m)	RPE(%)	APE (m)	RPE(%)	APE (m)	RPE(%)	APE (m)	RPE(%)	
FastLIO2	0.0117	0.0052	0.0294	0.0059	0.0200	0.0067	0.0341	0.0058	0.0299	0.0054	10
LIO-SAM	0.0180	0.0035	0.0305	0.0037	0.0189	0.0037	<b>0.0167</b>	0.0036	1.7142	0.0265	1000
LINS	0.0209	0.0239	0.0231	0.0257	0.0245	0.0270	0.0204	0.0227	1.6817	0.0528	3
LIKO (Ours)	<b>0.0091</b>	<b>0.0006</b>	<b>0.0198</b>	<b>0.0018</b>	<b>0.0180</b>	<b>0.0021</b>	0.0215	<b>0.0011</b>	<b>0.0245</b>	<b>0.0013</b>	1000

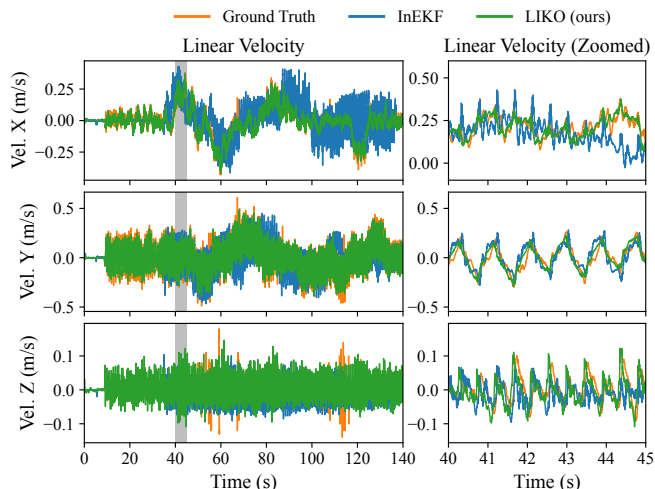


Fig. 4. *Left*: Linear velocity comparison between LIKO (green) and Contact-aided InEKF [8] (blue) against ground truth (orange). *Right*: Zoomed-in plot corresponding to the gray area of the left one. The more accurate and smoother velocity tracking allows for a better closed-loop control performance.

The accuracy result is shown in Table II. We achieve state-of-the-art evaluation accuracy in four of the five datasets. The only exception is on *walk\_in\_place*, where LIO-SAM and LINS show slightly higher accuracy than LIKO in APE. In the *up\_slope* dataset, LIO-SAM and LINS showed a great drift, while LIKO remains high accuracy. The reason is that the robot traversed uneven terrain in this dataset, and the leg odometry played a key role in such circumstances.

2) *Comparison with inertial-kinematic algorithms*: This section compares the LIKO against state-of-art Kinematic-Inertial odometry, contact-aided InEKF [8]. Since the position is unobservable for proprioceptive odometry, we only compare the linear velocity estimation of two algorithms, the result is shown in Fig. 4. The velocity ground truth was obtained by taking the time derivative of the MoCap data. A 20-data-wide sliding window filter was applied to the ground truth velocity to remove extra noise due to MoCap marker loss. It can be seen that LIKO achieves more accurate and smooth velocity estimation than contact-aided InEKF in the x and y directions. The robot’s velocity estimation in the z-direction is similar to that of the other two directions due to walking on flat ground with less disturbance.

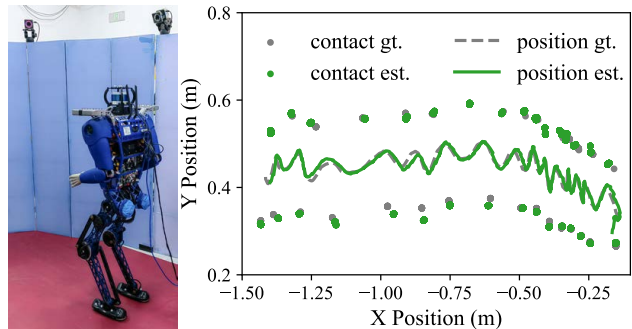


Fig. 5. *Left*: BHR-B3 walking in the MoCap room. Head and feet are equipped with MoCap markers. *Right*: Top-down view of the trajectory and contact position estimation (green) and the ground truth (gray). In the legend, "gt." stands for "ground truth" and "est." stands for "estimated".

#### D. Contact Position Estimation

The foot contact position estimation was also evaluated with MoCap Ground Truth, as shown in Fig. 5. MoCap markers are attached to the feet of the robot to measure contact position during locomotion. It can be seen that the LIKO provides an accurate estimation of the foot contact position. Note that the contact point in the graph is enlarged for better visualization and each contact position contains all of the points in its phase. This estimation can be used as feedback for the foothold plan and control module, providing a more robust locomotion behavior.

#### V. CONCLUSIONS

We have presented LIKO, a tightly coupled LiDAR-inertial-kinematic biped robot state estimation algorithm with online foothold estimation. Extensive experiments on the biped robot platform have shown that our algorithm outperforms many existing LiDAR-inertial or inertial-kinematic state estimation methods. The source code and dataset will be open-sourced to benefit the community.

We believe that LIKO’s accuracy will further improve with more detailed modeling of flat foot contact and kinematic parameters [32] addressed. In the future, we plan to develop corresponding downstream control applications and introduce visual sensors to help our robot conquer more challenging environments.

## REFERENCES

- [1] David Wisth, Marco Camurri, and Maurice Fallon. Vilens: Visual, inertial, lidar, and leg odometry for all-terrain legged robots. *IEEE Transactions on Robotics*, 39(1):309–326, 2022.
- [2] Yeting Liu, Junjie Shen, Jingwen Zhang, Xiaoguang Zhang, Taoyuanmin Zhu, and Dennis Hong. Design and control of a miniature bipedal robot with proprioceptive actuation for dynamic behaviors. In *2022 International Conference on Robotics and Automation (ICRA)*, pages 8547–8553. IEEE, 2022.
- [3] Min Sung Ahn. *Development and Real-Time Optimization-based Control of a Full-sized Humanoid for Dynamic Walking and Running*. University of California, Los Angeles, 2023.
- [4] Lei Wang, Libo Meng, Ru Kang, Botao Liu, Sai Gu, Zhihao Zhang, Fei Meng, and Aiguo Ming. Design and dynamic locomotion control of quadruped robot with perception-less terrain adaptation. *Cyborg and Bionic Systems*, 2022.
- [5] Marco Camurri, Milad Ramezani, Simona Nobili, and Maurice Fallon. Pronto: A multi-sensor state estimator for legged robots in real-world scenarios. *Frontiers in Robotics and AI*, 7:68, 2020.
- [6] Michael Bloesch, Christian Gehring, Péter Fankhauser, Marco Hutter, Mark A Hoepflinger, and Roland Siegwart. State estimation for legged robots on unstable and slippery terrain. In *2013 IEEE/RSJ International Conference on Intelligent Robots and Systems*, pages 6058–6064. IEEE, 2013.
- [7] Michael Bloesch. *State estimation for legged robots-kinematics, inertial sensing, and computer vision*. PhD thesis, ETH Zurich, 2017.
- [8] Ross Hartley, Maani Ghaffari, Ryan M Eustice, and Jessy W Grizzle. Contact-aided invariant extended kalman filtering for robot state estimation. *The International Journal of Robotics Research*, 39(4):402–430, 2020.
- [9] Wei Xu, Yixi Cai, Dongjiao He, Jiarong Lin, and Fu Zhang. Fast-lio2: Fast direct lidar-inertial odometry. *IEEE Transactions on Robotics*, 38(4):2053–2073, 2022.
- [10] Michael Bloesch, Marco Hutter, Mark A Hoepflinger, Stefan Leutenegger, Christian Gehring, C David Remy, and Roland Siegwart. State estimation for legged robots-consistent fusion of leg kinematics and imu. *Robotics*, 17:17–24, 2013.
- [11] Gerardo Bleidt, Matthew J Powell, Benjamin Katz, Jared Di Carlo, Patrick M Wensing, and Sangbae Kim. Mit cheetah 3: Design and control of a robust, dynamic quadruped robot. In *2018 IEEE/RSJ International Conference on Intelligent Robots and Systems (IROS)*, pages 2245–2252. IEEE, 2018.
- [12] Fabio Elneceave Xavier, Guillaume Burger, Marine Pétriaux, Jean-Emmanuel Deschaud, and François Goulette. Multi-imu proprioceptive state estimator for humanoid robots. *arXiv preprint arXiv:2307.14125*, 2023.
- [13] David Wisth, Marco Camurri, and Maurice Fallon. Robust legged robot state estimation using factor graph optimization. *IEEE Robotics and Automation Letters*, 4(4):4507–4514, 2019.
- [14] Maurice F Fallon, Matthew Antone, Nicholas Roy, and Seth Teller. Drift-free humanoid state estimation fusing kinematic, inertial and lidar sensing. In *2014 IEEE-RAS International Conference on Humanoid Robots*, pages 112–119. IEEE, 2014.
- [15] Shuo Yang, Zixin Zhang, Zhengyu Fu, and Zachary Manchester. Cerberus: Low-drift visual-inertial-leg odometry for agile locomotion. In *2023 IEEE International Conference on Robotics and Automation (ICRA)*, pages 4193–4199. IEEE, 2023.
- [16] Sangli Teng, Mark Wilfried Mueller, and Koushil Sreenath. Legged robot state estimation in slippery environments using invariant extended kalman filter with velocity update. In *2021 IEEE International Conference on Robotics and Automation (ICRA)*, pages 3104–3110. IEEE, 2021.
- [17] Paul J Besl and Neil D McKay. Method for registration of 3-d shapes. In *Sensor fusion IV: control paradigms and data structures*, volume 1611, pages 586–606. Spie, 1992.
- [18] Aleksandr Segal, Dirk Haehnel, and Sebastian Thrun. Generalized-icp. In *Robotics: science and systems*, volume 2, page 435. Seattle, WA, 2009.
- [19] Ji Zhang and Sanjiv Singh. Loam: Lidar odometry and mapping in real-time. In *Robotics: Science and systems*, volume 2, pages 1–9. Berkeley, CA, 2014.
- [20] Tixiao Shan and Brendan Englot. Lego-loam: Lightweight and ground-optimized lidar odometry and mapping on variable terrain. In *2018 IEEE/RSJ International Conference on Intelligent Robots and Systems (IROS)*, pages 4758–4765. IEEE, 2018.
- [21] Yue Pan, Pengchuan Xiao, Yujie He, Zhenlei Shao, and Zesong Li. Mulls: Versatile lidar slam via multi-metric linear least square. In *2021 IEEE International Conference on Robotics and Automation (ICRA)*, pages 11633–11640. IEEE, 2021.
- [22] Wei Xu and Fu Zhang. Fast-lio: A fast, robust lidar-inertial odometry package by tightly-coupled iterated kalman filter. *IEEE Robotics and Automation Letters*, 6(2):3317–3324, 2021.
- [23] Kenny Chen, Ryan Nemirow, and Brett T Lopez. Direct lidar-inertial odometry: Lightweight lio with continuous-time motion correction. In *2023 IEEE International Conference on Robotics and Automation (ICRA)*, pages 3983–3989. IEEE, 2023.
- [24] Brett T Lopez. A contracting hierarchical observer for pose-inertial fusion. *arXiv preprint arXiv:2303.02777*, 2023.
- [25] Lianqiang Han, Xuechao Chen, Zhangguo Yu, Zhifa Gao, Gao Huang, Jintao Zhang, Kenji Hashimoto, and Qiang Huang. A heuristic gait template planning and dynamic motion control for biped robots. *Robotica*, 41(2):789–805, 2023.
- [26] Zhifa Gao, Xuechao Chen, Zhangguo Yu, Lianqiang Han, Jintao Zhang, and Gao Huang. Hybrid momentum compensation control by using arms for bipedal dynamic walking. *Biomimetics*, 8(1):31, 2023.
- [27] Justin Carpentier, Nicolas Mansard, Florian Valenza, Joseph Mirabel, Guilhem Saurel, and Rohan Budhiraja. Pinocchio - Efficient and versatile Rigid Body Dynamics algorithms, July 2021.
- [28] Morgan Quigley, Ken Conley, Brian Gerkey, Josh Faust, Tully Foote, Jeremy Leibs, Rob Wheeler, Andrew Y Ng, et al. Ros: an open-source robot operating system. In *ICRA workshop on open source software*, volume 3, page 5. Kobe, Japan, 2009.
- [29] Tixiao Shan, Brendan Englot, Drew Meyers, Wei Wang, Carlo Ratti, and Rus Daniela. Lio-sam: Tightly-coupled lidar inertial odometry via smoothing and mapping. In *IEEE/RSJ International Conference on Intelligent Robots and Systems (IROS)*, pages 5135–5142. IEEE, 2020.
- [30] Chao Qin, Haoyang Ye, Christian E Pranata, Jun Han, Shuyang Zhang, and Ming Liu. Lins: A lidar-inertial state estimator for robust and efficient navigation. In *2020 IEEE International Conference on Robotics and Automation (ICRA)*, pages 8899–8906. IEEE, 2020.
- [31] Michael Grupp. evo: Python package for the evaluation of odometry and slam. <https://github.com/MichaelGrupp/evo>, 2017.
- [32] Shuo Yang, Howie Choset, and Zachary Manchester. Online kinematic calibration for legged robots. *IEEE Robotics and Automation Letters*, 7(3):8178–8185, 2022.